Measuring the Contributions of Basal Laminar Deposit and Bruch's Membrane in Age-Related Macular Degeneration

Amol A. Sura,[1] Ling Chen,[1,2] Jeffrey D. Messinger,[1] Thomas A. Swain,[1,3] Gerald McGwin Jr.,[1,3] K. Bailey Freund,[4–8] and Christine A. Curcio[1]

[1]Department of Ophthalmology and Visual Sciences, University of Alabama at Birmingham School of Medicine, Birmingham, Alabama, United States
[2]The First Affiliated Hospital of Chongqing Medical University, Chongqing Key Laboratory of Ophthalmology, and Chongqing Eye Institute, Chongqing, China
[3]Department of Epidemiology, School of Public Health, University of Alabama at Birmingham, Birmingham, Alabama, United States
[4]Vitreous Retina Macula Consultants of New York, New York, New York, United States
[5]Department of Ophthalmology, Faculty of Medicine, University of Tsukuba, Ibaraki, Japan
[6]LuEsther T. Mertz Retinal Research Center, Manhattan Eye Ear and Throat Hospital, New York, New York, United States
[7]Department of Ophthalmology, NYU Langone School of Medicine, New York, New York, United States
[8]Columbia University College of Physicians and Surgeons, Harkness Eye Institute, New York, New York, United States

Correspondence: Christine A. Curcio, Department of Ophthalmology and Visual Sciences, EyeSight Foundation of Alabama Vision Research Laboratories, 1670 University Boulevard, Room 360, University of Alabama at Birmingham School of Medicine, Birmingham, AL 35294-0019, USA; christinecurcio@uabmc.edu.

AAS and LC are co-authors who contributed equally to this work.

Received: July 25, 2020
Accepted: October 12, 2020
Published: November 13, 2020

Citation: Sura AA, Chen L, Messinger JD, et al. Measuring the contributions of basal laminar deposit and Bruch's membrane in age-related macular degeneration. *Invest Ophthalmol Vis Sci.* 2020;61(13):19. https://doi.org/10.1167/iovs.61.13.19

Purpose. Basal laminar deposit (BLamD) is a consistent finding in age-related macular degeneration (AMD). We quantified BLamD thickness, appearance, and topography in eyes of aged donors with and without AMD and evaluated its relationship to other components of the retinal pigment epithelium-basal lamina/Bruch's membrane (RPE-BL-BrM) complex.

Methods. Donor eyes (n = 132) were classified as normal (n = 54), early to intermediate AMD (n = 24), geographic atrophy (GA; n = 13), and neovascular AMD (NV; n = 41). In high-resolution histology, we assessed RPE, BLamD, and BrM thicknesses and phenotypes at 3309 predefined locations in the central (foveal and perifovea) and superior (perifoveal) sections. Pre-mortem optical coherence tomography (OCT) imaging of a 90-year-old woman was compared to postmortem histopathology.

Results. In non-atrophic areas of AMD eyes, the RPE-BLamD is thick (normal = 13.7 µm, early-intermediate = 16.8 µm, GA = 17.4 µm, NV = 18.7 µm), because the BLamD is thick (normal = 0.3 µm, early-intermediate = 5.5 µm, GA = 4.1 µm, NV = 5.3 µm). RPE layer thickness is similar across these stages. Disease-associated variants of BLamD (thick, late, basal mounds) cluster subfoveally. A thick BLamD is visible on OCT as a hyporeflective split in the RPE-BL-BrM complex. BrM is thin (3.5 µm) in NV (normal = 4.2 µm, early to intermediate = 4.4 µm, and GA = 4.2 µm).

Conclusions. The RPE-BL-BrM complex is thick in AMD, driven by the accumulation and expansion of BLamD rather than expansion of either three-layer BrM, RPE-BL, or RPE. BLamD is clinically appreciable by OCT in some patients as a non-neovascular "split RPE-BL-BrM complex" or "double-layer sign." BLamD may contribute toward the formation and progression of high-risk drusen yet also exhibit protective properties.

Keywords: basal laminar deposit, basal laminar deposit (BLamD), age-related macular degeneration (AMD), age-related macular degeneration, histopathology, histology, retinal pigment epithelium, Bruch's membrane, basal linear deposit, drusen, optical coherence tomography (OCT), segmentation, neovascularization

Age-related macular degeneration (AMD) is the fourth largest cause of vision loss globally[1] as a consequence of macular neovascularization (MNV) and macular atrophy (MA) in its advanced forms. Although intravitreal injections of antivascular endothelial growth factor agents are the current standard of care for treating MNV,[2] some treated eyes ultimately lose central vision due to atrophy of the retinal pigment epithelium (RPE) and photoreceptors. Further, aside from nutritional supplements for a subset of patients,[3] there is no proven treatment for non-neovascular AMD or its advanced stage of geographic atrophy (GA).

Optical coherence tomography (OCT) has become the primary imaging modality used in the evaluation and

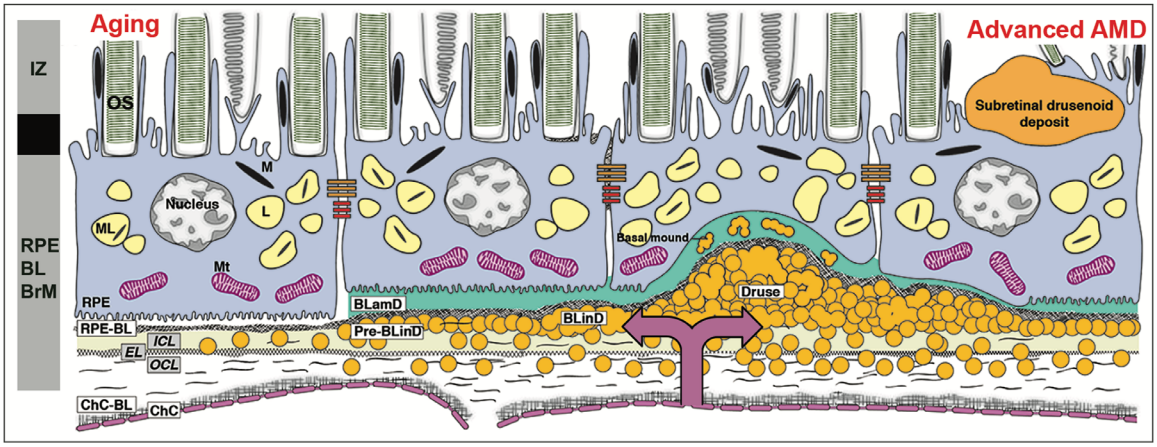

Figure 1. The layers of age-related macular degeneration include basal laminar deposit. The RPE as an epithelium rests on a basal lamina of extracellular matrix (at left).[4] BLamD is a stereotypically thickened extracellular matrix (*green, in middle and right*) between the RPE plasma membrane and this basal lamina. BLamD either replaces or incorporates the RPE basal infoldings, shown as *pleats at the bottom* of the RPE cell body at the left). The trilaminar Bruch's membrane (BrM)[5,15,34,96] consists of the inner collagenous layer (ICL), elastic layer (EL), and outer collagenous layer (OCL). Between the RPE basal lamina (or BLamD) and inner collagenous layer of Bruch's membrane (subRPE-BL space) accumulate soft drusen material (lipoprotein-related debris or "membranous debris")[15] and in some eyes type 1 MNV, of choroidal origin (*double headed arrow*). Soft druse material is found also in basal linear deposits (BLinD) and in basal mounds within BLamD.[17] BLinD may be continuous with, yet distinct from drusen, which are dome-shaped. The schematic bar at the left shows the third and fourth outer retinal reflective bands of currently available commercial optical coherence tomography[4] (OCT) with our interpretation based on recent mapping of RPE organelles[97,98] and supported by adaptive optics assisted OCT.[99,100] The third band, interdigitation zone (IZ), corresponds to interleaved photoreceptor outer segments and RPE apical processes with their notable content of melanosomes. Components of the fourth band include the RPE cell body, RPE basal infoldings, RPE-BL, BLamD if present, contents of sub-RPE-BL space if present, and ICL-EL-OCL of BrM. The apical 3/4 of the RPE cell body contains approximately 700 reflective lipofuscin and melanolipofuscin granules with some melanosomes and a similar number of reflective mitochondria in basolateral 3/4 (middle half has all organelles). The unnamed hyporeflective band between IZ and RPE-BL-BrM band are currently thought to be a zone of apical processes where they depart from the cell body and lack melanosomes.[98] An attribution to a layer of phagosomes within the RPE cell body based on selective stains was not supported by comprehensive electron microscopy.[101] OS, outer segments of photoreceptors; RPE, retinal pigment epithelium; M, melanosome; ML, melanolipofuscin; Mt, mitochondria; RPE-BL, RPE basal lamina; BLamD, basal laminar deposit; BLinD, basal linear deposit; ChC, choriocapillaris; ChC-BL, ChC basal lamina.

management of all forms of AMD. OCT reveals the three-dimensional microstructure of both MNV precursors and outer retinal features leading to MA. The fourth outer retinal hyper-reflective band seen with commercially available spectral domain and swept source OCT devices is called the RPE-Bruch's membrane (BrM) complex in consensus nomenclature.[4] Because this band includes RPE cell bodies + basal lamina of the RPE (RPE-BL) + the remaining layers of BrM (Fig. 1), we use the term RPE-BL-BrM complex. Like others,[5,6] we have found that AMD is best understood when BrM is defined by its middle three layers, rather than all five layers. This definition allows a separate role in AMD progression for the RPE-BL.

RPE adherence to an underlying BL is typical of all epithelial cells. Basal laminae are the main element of basement membranes, which separate epithelial cells from an underlying stroma (i.e. BrM) and provide an enzymatic substrate for anti-angiogenesis, cell-signaling, and inflammation.[7–9] RPE-BL expresses specialized collagen IV isoforms like kidneys.[10] In AMD, a stereotypic deposition of basement membrane material called basal laminar deposit (BLamD) accumulates internal to the RPE-BL, either replacing or incorporating the RPE basal infoldings (see Fig. 1). BLamD shares features with basement membranes. It tightly binds the RPE, stains for carbohydrates, and contains basement membrane proteins like laminins, fibronectin, plus wide-spaced type VI collagen. This matrix also contains epidermal growth factor-containing fibulin-like extracellular matrix protein 1 (EFEMP1), matrix metalloproteinase 7 (MMP7), tissue inhibitor of metalloproteinase 3 (TIMP3), complement factors, and glycoproteins.[11–14]

The presence and abundance of histologic BLamD under the fovea was used to define AMD presence and severity by S.H. Sarks. By electron microscopy, she definitively separated BLamD from soft drusen material (see Fig. 1).[15] Inconsistent early nomenclature for two deposits (Table 1), basal laminar and basal linear (BLinD, soft druse material; see Fig. 1), was resolved by W.R. Green, who retained the two names,[16] as do we. In surveying 107 clinically documented AMD eyes, S.H. and J.P. Sarks showed that thick BLamD, often with a late-appearing scalloped morphology, was accompanied by poor visual acuity and RPE dysmorphia.[17] In addition, the presence of BLamD was a prerequisite for the appearance of soft drusen material, in any form, including basal mounds (BMounds) within its substance (see Fig. 1).

To inform OCT interpretation of the RPE-BL-BrM complex and refine models of AMD pathogenesis, we herein survey BLamD phenotypes and thicknesses in normal aged eyes and eyes with early to intermediate and advanced AMD. The Project MACULA online histopathology resource provides macula-wide submicrometer epoxy sections to accurately delineate BLamD from BLinD and BrM over a larger sample area than that studied by the Sarks. We preserve retinal topography, because recent evidence indicates that two major risk factors for progression, soft drusen, and subretinal drusenoid deposits, follow the topography of cone and rod photoreceptors, respectively.[18] In an eye with clinical

Investigative Ophthalmology & Visual Science

Table 1. Evolution of the Nomenclature for Basal Laminar Deposit (BLamD) and Basal Linear Deposit (BLinD)*

	Gass[102]	Sarks[37]	Feeney-Burns[44]	Sarks[103] Green[16] Van der Schaft[39] Curcio[48]	**Curcio[45,54]	Curcio[18,104]
Internal to RPE-BL	Eosinophilic granular deposits	Basal linear deposit	Secretory deposit	Basal laminar deposit	Basal deposits	Basal laminar deposit
External to RPE-BL	Drusen	Drusen	Linear basal deposit and soft drusen	Basal linear deposit and drusen	Basal deposits	Basal linear deposit and drusen

* The term basal laminar drusen[105] has been superseded by cuticular drusen, which are identical to hard drusen by histopathology.[106]
RPE-BL, retinal pigment epithelium basal lamina.
The term basal deposits should be avoided as a shorthand term for all the layers between the RPE plasma membrane and the inner collagenous layer of Bruch's membrane if transmission electron microscopy or high-resolution light microscopy views of epoxy-embedded tissue[48] are available. A more appropriate term is sub-RPE deposits.

imaging acquired before patient death, we investigate whether BLamD can be visualized with commercial OCT devices as a hyporeflective spitting of the RPE-BL-BrM complex, sometimes called the "double layer sign." Because 15% of eyes with early to intermediate AMD have nonexudative type 1 MNV,[19] distinguishing a double layer sign due to thick BLamD from MNV in vivo may ultimately assist management decisions. We confirm BLamD expansion as a major change to the RPE-BL-BrM complex in early AMD and the importance of thick BLamD as a risk factor for disease progression, especially in the central macula.

Methods

Compliance

The institutional review board at the University of Alabama at Birmingham approved this study. All procedures adhered to the tenets of the Declaration of Helsinki and the Health Insurance Portability and Accountability Act.

Overview of Design Choices for Project MACULA

Project MACULA (https://projectmacula.org/) is an online digital microscope with high-resolution histology and annotated layer thickness of human donor eyes with and without AMD. A premise behind its creation was that accurate depiction and quantification of cell and tissue features in histology could leverage longitudinally tracked OCT in clinical trial image datasets and practices with long-standing OCT usage to generate a cellular-level timeline of disease. A timeline can refine models of pathogenesis and therapeutic strategies and is uniquely possible in precisely layered retina. Another premise is that prominent pathology in the RPE-BL-BrM complex is related to the physiology of cells in the overlying retina.

Our methods were driven by the requirements of validating OCT imaging of the RPE-BL-BrM complex. Reflectivity is largely generated via Mie scattering from aqueous-lipid interfaces, such as organelles. We sought subcellular resolution and comprehensive histology of tissue elements in all chorioretinal layers. We used an electron microscopy preparation (i.e. osmium tannic acid paraphenylenediamine post-fixation and epoxy-resin-embedded submicrometer sections viewed and scanned with oil-immersion light microscopic objectives to expand sample size). This post-fixation method stains lipids well and imparts polychromasia to toluidine blue stained sections (compare to reference 20). Whole slide scanning allowed seamless multiscale viewing between low magnification for context and high magnification for details.

Our approach can be compared to paraffin sections and cryo-sections (5 and 10–20 µm thick, respectively). These are excellent for molecular characterization via immunohistochemistry but have lower spatial resolution and may mislead if sections are not strictly orthogonal to BrM due to projection imaging of tilted layers. Our approach also can be compared with fluorescence microscopy for selective markers, which may also mislead if not accompanied by a comprehensive visualization technique (e.g. brightfield image of an adjoining section) to indicate nonlabeled tissue elements.

Histology Preparation

Eyes were accessioned from white, nondiabetic donors by the Alabama Eye Bank between 1995 and 2012 in 2 tranches.[21] Ophthalmic histories were not available. Eyes with neovascular AMD were largely accessioned before 2006 (the era of anti-anti-vascular endothelial growth factor therapy) and may have received treatments available during that period. Eyes collected from 1995 to 2010 and not used for specific studies were retained in fixative. During the period 2011 to 2012, fellow eyes to those collected for an RNA-sequencing project were retained for histologic evaluation.[22] All eyes were preserved in 1% paraformaldehyde and 2.5% glutaraldehyde in a 0.1M phosphate buffer with an average death-to-preservation time of 3:49 (range = 0:40–11:40). Prior to histology, all eyes were subjected to ex vivo imaging with color fundus photography and OCT as described[21]; these imaging data are available on the website but are not reported here.

Macula-wide, full-thickness tissue punches were obtained with an 8.25 mm diameter trephine (#68825-L; Howard Instruments, Tuscaloosa, AL, USA). Punches were post-fixed with osmium tannic acid paraphenylenediamine to highlight neutral extracellular lipids.[23] After embedding in epoxy resin, tissues were sectioned at 0.8 µm starting at the superior edge of the punch, as indexed by the microtome counter, and stained with toluidine blue. One group of sections was taken at approximately 2 mm from this starting point to capture the rise of rod density in superior perifovea. Another group was taken at approximately 4 mm from the top to capture the rod-free zone, as determined by inspection of stained preliminary sections. Final sections at each of two locations (superior and central) were scanned along their entire length and digitized using image stitching software (CellSens; Olympus).

Table 2. Baseline Characteristics of Donor Eyes

Histologic Diagnosis	Donors	Age	Female, n / %	Total Sections	Central	Superior	Locations	Locations Per Eye
Unremarkable	54	79.7 ± 9.9	29 / 53.7	97	52	45	1364	25
Early-intermediate AMD	24	82.4 ± 8.5	17 / 70.8	32	23	9	515	22
Geographic atrophy	13	85.4 ± 4.7	9 / 69.2	24	11	13	336	25
Neovascular AMD	41	84.9 ± 7.2	26 / 63.4	77	40	37	1094	27

Histologic Diagnosis

AMD was defined as drusen larger than 125 µm or severe RPE dysmorphia in the setting of drusen or basal linear deposit, in both cases, with or without neovascularization and sequelae. Early to intermediate non-neovascular AMD was defined as having one druse > 125 µm in width; GA was defined as absence of a continuous RPE layer > 250 µm.[21] The resulting four diagnostic groups (see Results) have many samples but are not balanced, due to how eyes were collected, and because some eyes with GA ($n = 11$) and large drusen ($n = 9$) accessioned during this period were used for other studies.

Assaying Layer Thicknesses and Phenotypes Within Macular Topography

AMD deposits and deposit-related progression risk track the topography of macular photoreceptors, which are radially organized around the foveal singularity.[18,24] High-risk drusen and BLinD are concentrated in central macula,[18,25,26] where foveal cones and Müller glia are numerous. Like rods, subretinal drusenoid deposit is abundant along an elliptical ring surrounding the optic nerve head and macula.[27] We accommodated this geometry with tissue sections that are parallel to a line through the fovea and optic nerve head. We used a central section that included the rod-free zone of the fovea, flanked by the nasal and temporal perifovea, and a superior section that included only superior perifovea. Both sections were aligned on a vertical line through the foveal center (Table 2). Analysis was limited to sites ≤ 2.0 mm in a nasal and temporal direction from this center to account for variable centration of original tissue punches around the fovea and to exclude peripapillary locations where BLamD has a distinct morphology. Central sections were sampled 2.0 mm, 1.5 mm, 1.0 mm, 0.8 mm, 0.6 mm, 0.4 mm, 0.2 mm, 0.1 mm, 0.05 mm, and 0 mm nasal and temporal to the foveal center (i.e. more locations in the fovea where photoreceptor densities exhibit steep gradients). Superior sections were sampled 2.0 mm, 1.5 mm, 1.0 mm, 0.6 mm, and 0 mm nasal and temporal to the section center. Because photoreceptor density gradients are flatter than they are in the fovea, fewer locations were used.

At each sampled location, RPE, BLamD, and BrM thicknesses were measured by one observer (author C.A.C.) with custom software ("M&A" plug-in, ImageJ[28]), guided by the three-layer BrM shown in Figure 1. RPE atrophy was defined as locations where RPE thickness was 0 in the absence of tissue preparation artifact. BLamD phenotypes were assigned by one observer (author C.A.C.). BLamD phenotypes (to be illustrated in the Results section) were nonmutually exclusive and selected from a drop-down menu that included: early, late, thick, basal mounds, and persistent.[17] For this report, data generated from these categorical assessments will be capitalized, and use of these terms as descriptors will be noncapitalized. Early BLamD was blue staining "palisades" often resembling fingerprints.[17] Late BLamD was dense with multiple scalloped layers that were concave toward BrM. Thick BLamD was defined as > 6.2 µm, which represents half the thickness of the average RPE cell body.[29] Late BLamD was defined as dense and scalloped. BMounds were defined as soft druse material within BLamD.[17] Persistent BLamD was present in the absence of RPE[17] and continuous with other BLamD phenotypes. RPE phenotypes were independently assigned by two observers, masked to each other's grades, according to the 2015 Project Macula RPE classification.[21,30] Locations where RPE thicknesses were 0 in the absence of tissue preparation artifact were considered RPE atrophy. For topographic evaluation, Fovea was defined as ≤ 0.6 mm of the foveal center. Nasal and temporal perifovea was defined as 0.6 to 2.0 mm from the foveal center in the appropriate direction. Superior perifovea was defined as any location within the superior section.

Clinically Documented Case

Comprehensive ophthalmic examination, including multimodal imaging, was performed during a 9-year follow-up for a woman of European descent who presented at age 79 years with bilateral AMD. The left eye was used for this study. Ocular history included bilateral cataract surgery. Medical history included chronic obstructive pulmonary disease (COPD), gastric cancer, and hypercholesterolemia. There was a 57 pack-year history of smoking. At presentation, inactive subretinal fibrosis was noted in the right eye. Nonexudative type 1 MNV manifest as late staining on fluorescein angiography was present in the left eye. Best-corrected visual acuity (BCVA) at baseline was 20/50 in the right eye and 20/25 in the left eye. The first near-infrared reflectance (NIR) and spectral domain OCT images (Heidelberg Spectralis HRA + OCT; Heidelberg Engineering, Heidelberg, Germany) were acquired 10 months after presentation and showed a large shallow irregular RPE elevation (SIRE) in the left eye without evidence of exudation. During follow-up, neither eye received treatment for neovascular AMD. At the last clinical evaluation, OCT showed no evidence of macular exudation in either eye, and a persistent subfoveal SIRE in the left eye. BCVA was 20/200 in the right eye and 20/30 in the left eye. Sixteen months later, the patient died of complications of COPD at age 90 years. Eyes were recovered 6.25 hours after death by personnel of The Eye-Bank for Sight Restoration (New York, NY, USA), opened anteriorly by corneal excision, preserved by immersion in 4% phosphate buffered paraformaldehyde, and shipped overnight on wet ice to Birmingham, AL, USA. Descriptions of subretinal drusenoid deposits and nonexudative type 1 MNV in this eye have been reported.[19,31]

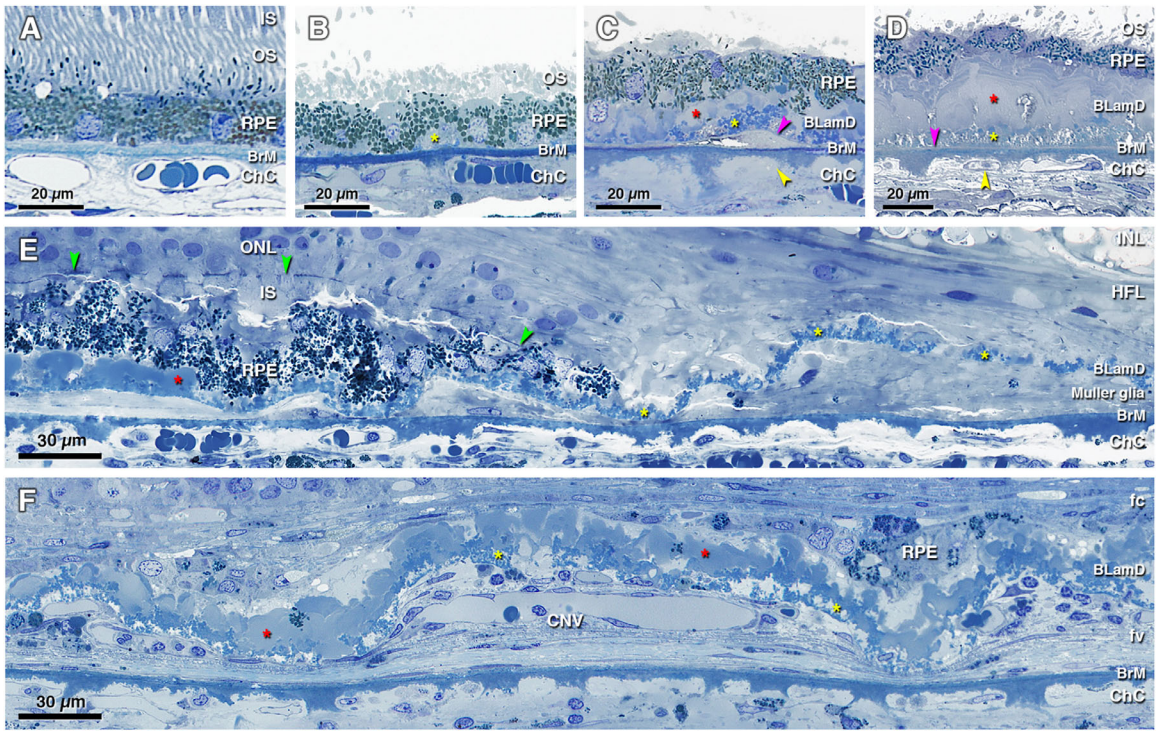

Figure 2. Histopathology of basal laminar deposits (BLamD) in age-related macular degeneration (AMD). (**A**) Normal macula, without BLamD in a 77-year-old woman, 2000 µm nasal to the foveal center. (**B**) Patchy early BLamD (*yellow asterisk*) in a normal macula in an 88-year-old man, 600 µm nasal. (**C**) Early (*yellow asterisk*) and late (*red asterisk*) BLamD, along with basal linear deposit (fuchsia arrowhead), in an 85-year-old woman with early to intermediate AMD. *Yellow arrowhead*, ChC ghost, 400 µm temporal. (**D**) Thick, continuous early and late BLamD (*yellow and red asterisks*) in an 88-year-old man with early to intermediate AMD. A thin layer of pre-BLinD (*fuchsia arrowhead*) can be observed in this eye. *Yellow arrowhead*, ChC retraction, 290 µm nasal. (**E**) Persistent BLamD in the atrophic zone (*yellow asterisks*) of a 76-year-old woman with geographic atrophy. Müller glial processes were observed in the sub RPE-BL space. Note the continuity of BLamD across the border of atrophy, signified by the descent of the external limiting membrane (*green arrowheads*), 400 µm nasal. (**F**) Persistent BLamD overlying choroidal neovascularization (CNV) in a 91-year-old female. Both early and late (*yellow and red asterisks*) BLamD can be observed. Fibrovascular (fv) and fibrocellular (fc) membranes are shown on either side of the persistent BLamD, 490 µm temporal. INL, inner nuclear layer; HFL, Henle fiber layer; ONL, outer nuclear layer; IS, inner segment; OS, outer segment; RPE, retinal pigment epithelium; BrM, Bruch's membrane; ChC, choriocapillaris. Retina is detached from RPE in panels **B** to **D**.

Quantitative Analysis

Data are presented as percentage of eyes affected with various features. For layer thicknesses, values from different locations within the same eye are presented as medians and interquartile ranges (Excel version 16.38; Microsoft, Redmond, WA, USA)

Results

Results are based on 3309 sample locations from 132 eyes (22–27 locations per eye, depending on the diagnostic group). Donor characteristics are shown in Table 2. In total, there were 54 normal maculae without AMD, 24 maculae with early to intermediate AMD, 13 maculae with GA, and 41 maculae with neovascular (NV) AMD.

Basal Laminar Deposit in AMD

Figures 2 and 3 demonstrate that the range of BLamD forms originally described by the Sarks are also visible in our material.[17] Early BLamD in normal, aged eyes usually appeared thin and patchy (see Fig. 2B). By contrast, all AMD eyes had extensive BLamD, which often included thick, continuous stretches of early BLamD underneath the fovea. BLamD sometimes took on a multilaminated appearance with early BLamD overlaid by thick, scalloped-appearing late BLamD (Fig. 2C, 2D). Although related to the RPE basal lamina, BLamD may persist even after RPE atrophy. This persistent BLamD was the predominant form of BLamD in GA (see Fig. 2E) and MA of NV AMD (see Fig. 2F). Of importance to a dysregulated transport model of AMD progression, Figures 2 and 3 also show many examples of choriocapillaris endothelium degeneration, including retraction and disappearance of endothelium from the arches of BrM intercapillary pillars ("ghosts").[32–34]

Another notable feature of BLamD was the presence of BMounds (see Fig. 3). These accumulations of soft druse material (lipoprotein-derived debris) within BLamD were common in eyes with AMD (see Fig. 3). They differ from drusen and BLinD by their location. BMounds, like BLamD, are internal to the basal lamina of the RPE cell, whereas drusen and BLinD are external to it (see Fig. 3A). BMounds appeared as solitary excrescences (see Fig. 3B) or as a semicontinuous horizontal layer at the base of BLamD (see

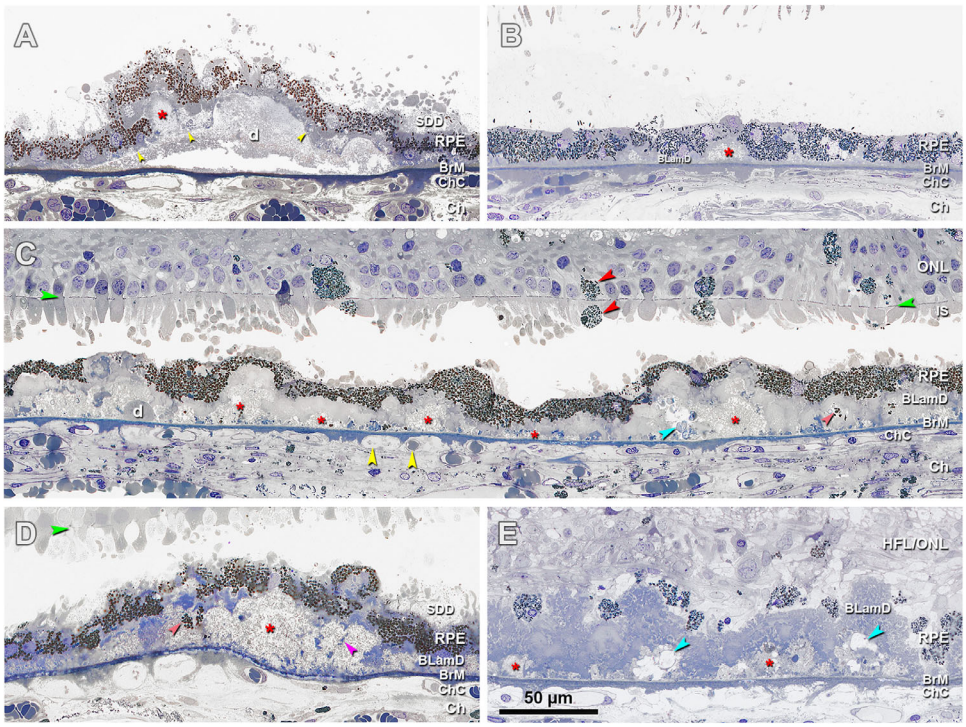

Figure 3. Histopathology of basal mounds (BMounds) in age-related macular degeneration (AMD). (**A**) BMounds (*red asterisk*) are internal to the RPE basal lamina (*yellow arrowhead*) whereas drusen (d) are external to it, in a 76-year-old woman with early to intermediate AMD, 200 µm nasal. (**B**) BMounds (*red asterisk*) may appear as focal mound-like excrescences, in a 95-year-old man with early to intermediate AMD, 400 µm nasal. (**C**) BMounds (*red asterisk*) may form a semicontinuous layer of lipoprotein rich material within the BLamD. Pigmented cells of RPE origin can be observed in the retina and subretinal space (*red arrowheads*). *Yellow arrowheads*, retracted ChC and ghosts, in an 83-year-old woman with outer retinal atrophy, 1500 µm nasal. (**D**) BMounds can become quite large (*red asterisk*) and include complex features, such as internal structure (*fuchsia arrowhead*) and non-nucleated granule aggregates shed from RPE (*orange arrowhead*) in an 85-year-old woman with early to intermediate AMD, 1500 µm temporal. (**E**) Much like drusen, BMounds (*red asterisk*) may become calcified (*blue arrowhead*) in a 96-year-old woman with early to intermediate AMD, 2000 µm temporal. HFL, Henle fiber layer; ONL, outer nuclear layer; HFL/ONL, dyslamination of HFL and ONL; IS, inner segment; RPE, retinal pigment epithelium; BLamD, basal laminar deposit; BrM, Bruch's membrane; Ch, choroid; ChC, choriocapillaris. *Green arrowhead*, external limiting membrane. SDD, subretinal drusenoid deposits; Retina is detached from RPE in panels **A** to **D**.

Fig. 3C). Like soft drusen, BMounds also exhibited calcification (see Fig. 3E). Notably Bmounds sequestered granule aggregates shed from the RPE (see Fig. 3D).

Measurements of BLamD reinforce its omnipresence in AMD (Fig. 4; see Fig. 5). Although the majority (74.1%) of normal eyes had some BLamD, it was patchy and encountered in only 24% of sampled locations. All eyes with early to intermediate AMD and 97.6% (40/41) of eyes with NV AMD had some BLamD, and when present, it was encountered frequently (% of sampled locations: early to intermediate = 80.6%, GA = 84.8%, and NV = 71.0%; see Fig. 4). As shown in Figure 5 and Table 2, median BLamD thickness was 0.3 µm in normal eyes, whereas it was 5.5 µm in early to intermediate, 4.1 µm in GA, and 5.5 µm in NV. Eyes with higher degrees of RPE dysmorphia displayed thick BLamD (Table 3).

In eyes with AMD, BLamD was widely distributed across all assessed locations, and the subtypes indicative of progression,[17] thick BLamD, late BLamD, and BMounds, were highest under the fovea (Fig. 6). Of interest, because epidemiologic studies have shown that high-risk drusen cluster under the fovea, we found that BMounds, which contain soft drusen material, are frequent in this region in normal eyes and infrequent in other regions (Fig. 6).

The RPE-BL/Bruch's Membrane Complex

In non-atrophic locations (locations with non-zero RPE thickness), normal, early to intermediate, GA, and NV eyes had similarly thick layer of RPE cell bodies (12.5 µm, 11.2 µm, 12.7 µm, and 13.6 µm, respectively; see Fig. 5; Table 4). As AMD progresses, the distribution of RPE cell body morphologies shifts toward abnormal (Fig. 7; Supplementary Table S1). Neovascular AMD eyes contained thin BrM (3.5 µm), compared to normal (4.2 µm), early to intermediate AMD (4.4 µm), and GA eyes (4.2 µm; see Fig. 5; Table 4).

Because the RPE-BL complex is indivisible by spectral domain and swept source OCT, we measured the thickness of the RPE-BL complex in areas where the RPE was present (Fig. 5; Table 4; normal = 13.7 µm [12.5–14.9], early to intermediate = 16.8 µm [15.0–19.8], GA = 17.4 µm [15.4–21.8], and NV = 18.7 µm [15.3–23.2]). When all locations were sampled, this complex was thin in advanced disease relative to early to intermediate AMD due to large areas of RPE atrophy. It was not zero, due to large areas of persistent BLamD. To assess the distance between the RPE cell bodies and choriocapillaris endothelium, the thickness of BLamD plus BrM was computed. This thickness was 4.4 µm in normal

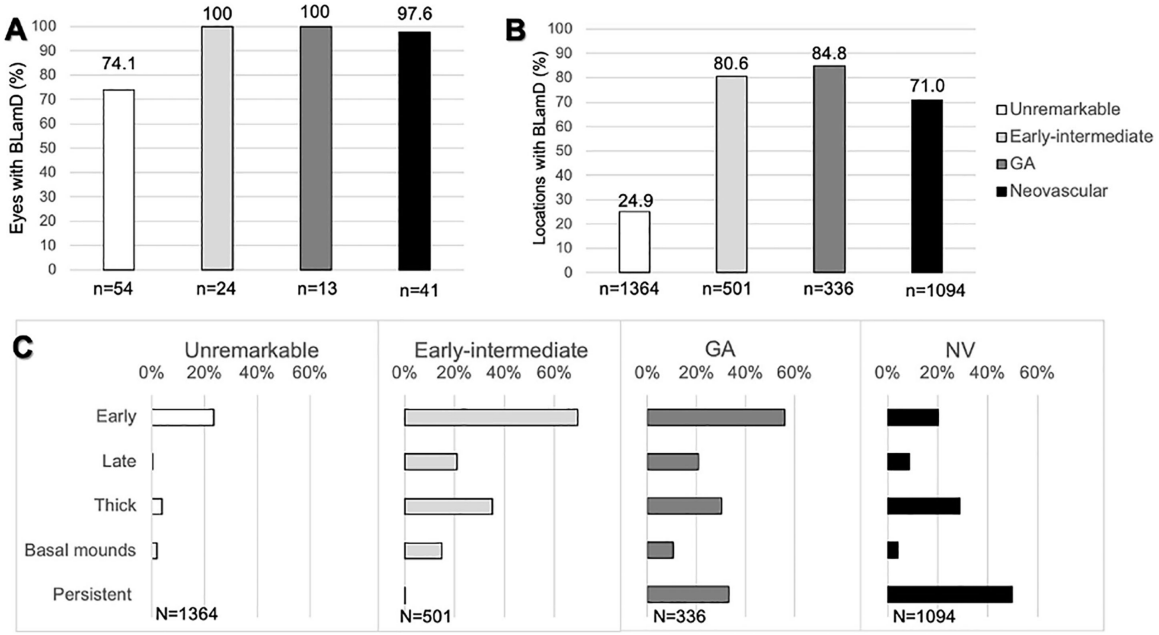

Figure 4. Basal laminar deposit (BLamD) is ubiquitous in age-related macular degeneration (AMD). At predefined locations in the fovea and perifovea, the presence of BLamD was assayed (19–38 locations per eye) and morphologic phenotype defined. (**A**) Most aged eyes had at least one location with BLamD. (**B**) When locations are systematically sampled, BLamD is more commonly encountered in AMD. (**C**) BLamD phenotypes shift along different diagnostic classes of AMD. Although a feature of normal aging, early BLamD considerably accumulates in early to intermediate AMD and geographic atrophy (GA). Thick BLamD (defined as BLamD half as thick as the average RPE cell [> 6.2 µm]) and late BLamD were associated with the transition to early-intermediate AMD. Basal mounds—drusen-like accumulations of lipid within BLamD—were likewise more common in eyes with AMD. Persistent BLamD are found in areas of atrophy and represent a predominant form of BLamD in GA and neovascular AMD.

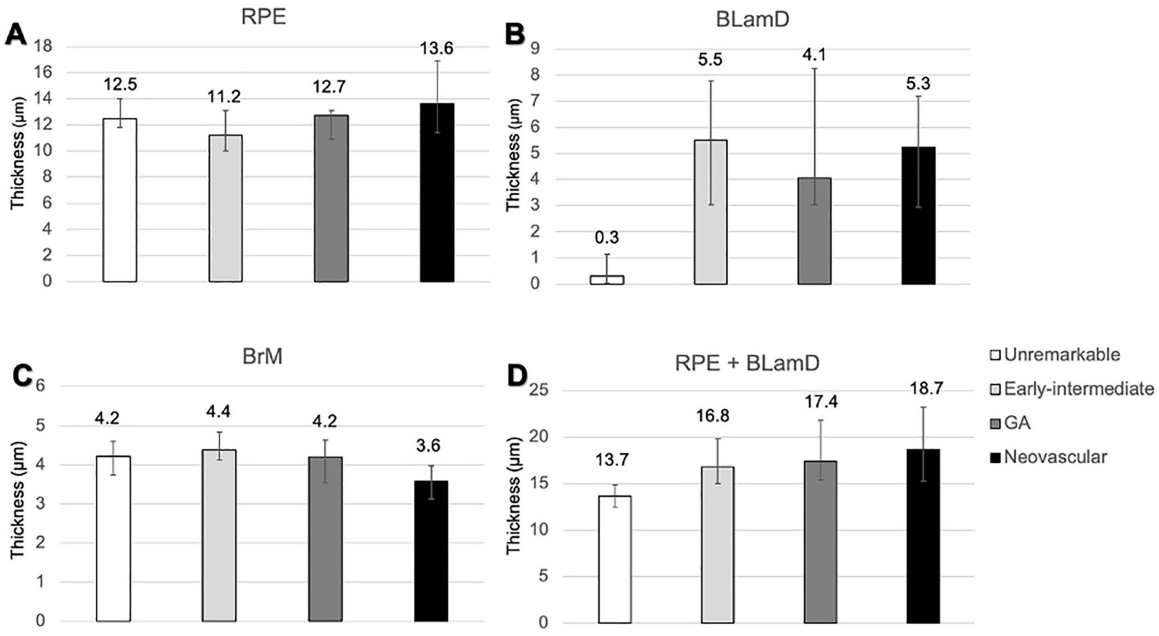

Figure 5. Thickness of the retinal pigment epithelium (RPE), basal laminar deposit (BLamD), and Bruch's membrane (BrM) in different stages of age-related macular degeneration (AMD). At predefined locations in the fovea and perifovea, RPE, BLamD, and BrM were assayed (19–38 locations per eye). Only nonzero RPE measurements were included. Measurements within the same eye were averaged, and each eye was ranked. Data represent median and interquartile range of the rank list. (**A**) RPE cell body thicknesses were similar between groups with more variability in advanced disease. (**B**) Eyes with AMD strikingly accumulate BLamD compared to eyes without disease. (**C**) The interquartile range of BrM thicknesses was thin in neovascular AMD (3.1–4.0), relative to normal (4.1–4.8), and early to intermediate AMD (4.0–4.6). (**D**) The median RPE + BLamD was 3 to 5 µm greater in AMD eyes relative to normal eyes. The thickening of the RPE-basal lamina/BrM complex in AMD is largely driven by the addition and expansion of BLamD.

Table 3. Thickness of Basal Laminar Deposit (BLamD) in Relation to Retinal Pigment Epithelium (RPE) Phenotypes

	Unremarkable		Early to Intermediate		Geographic Atrophy		Neovascular AMD		Overall	
RPE Phenotypes	**BLamD Thickness (µm)**	**N**	**BLamD Thickness (µm)**	**N**	**BLamD Thickness (µm)**	**N**	**BLamD Thickness (µm)**	**N**	**BLamD Thickness (µm)**	**N**
Normal aging	0	1158	0 (0, 2.9)	147	1.1 (0, 2.1)	45	1.6 (0, 3.1)	19	0 (0, 0)	1369
Very non-uniform	3.3 (0, 5.4)	184	4.6 (2.6, 8.3)	237	4.7 (2.6, 8.4)	100	3.9 (1.5, 7.6)	128	4.1 (1.9, 7.3)	649
Sloughing	0	2	6.7 (3.6,10.2)	40	4.3 (3.2, 7.9)	26	6.0 (2.7, 8.1)	26	5.9 (3.1, 8.5)	94
Shedding	8.5 (6.6, 10.6)	4	12.2 (9.6, 17.7)	39	9.7 (7.2, 13.3)	35	11.3 (7.2, 15.7)	22	11.2 (7.6, 14.9)	101
Bilaminar	–	0	11.8	3	11.8	2	3.7 (7.2, 15.7)	24	4.0 (2.0, 7.7)	29
Vacuolated	–	0	11	2	0	1	3.9	2	4.9 (2.9, 10.5)	5
Intraretinal	–	0	5.5 (3.5, 8.2)	38	3.6	2	8.3 (4.1, 11.3)	15	5.6 (3.7, 9.0)	55
Atrophy with BLamD	–	0	8.5 (5.3,19.0)	7	4.1 (2.7, 5.3)	81	5.1 (3.3, 9.0)	240	4.8 (3.3, 8.35)	431
Atrophy without BLamD	–	0	–	0	0	14	0	214	0	231
Entombed	–	0	–		–	0	4.4 (2.1, 6.7)	262	4.4 (2.6, 6.7)	265
Dissociated	–	0	–	0	4.4 (2.8,7.2)	29	6.7 (3.8, 10.8)	32	5.4 (3.1, 9)	61
Overall	0.3 (0, 1.1)	1348	5.5 (3.1, 8.6)	513	4.1 (3.6, 7.0)		5.5 (3.1, 8.6)	1084		3290

At predefined locations in the fovea and parafovea, thicknesses of the RPE, BLamD, and BrM were assayed (19–38 locations per eye). Data are presented as the median and interquartile range.

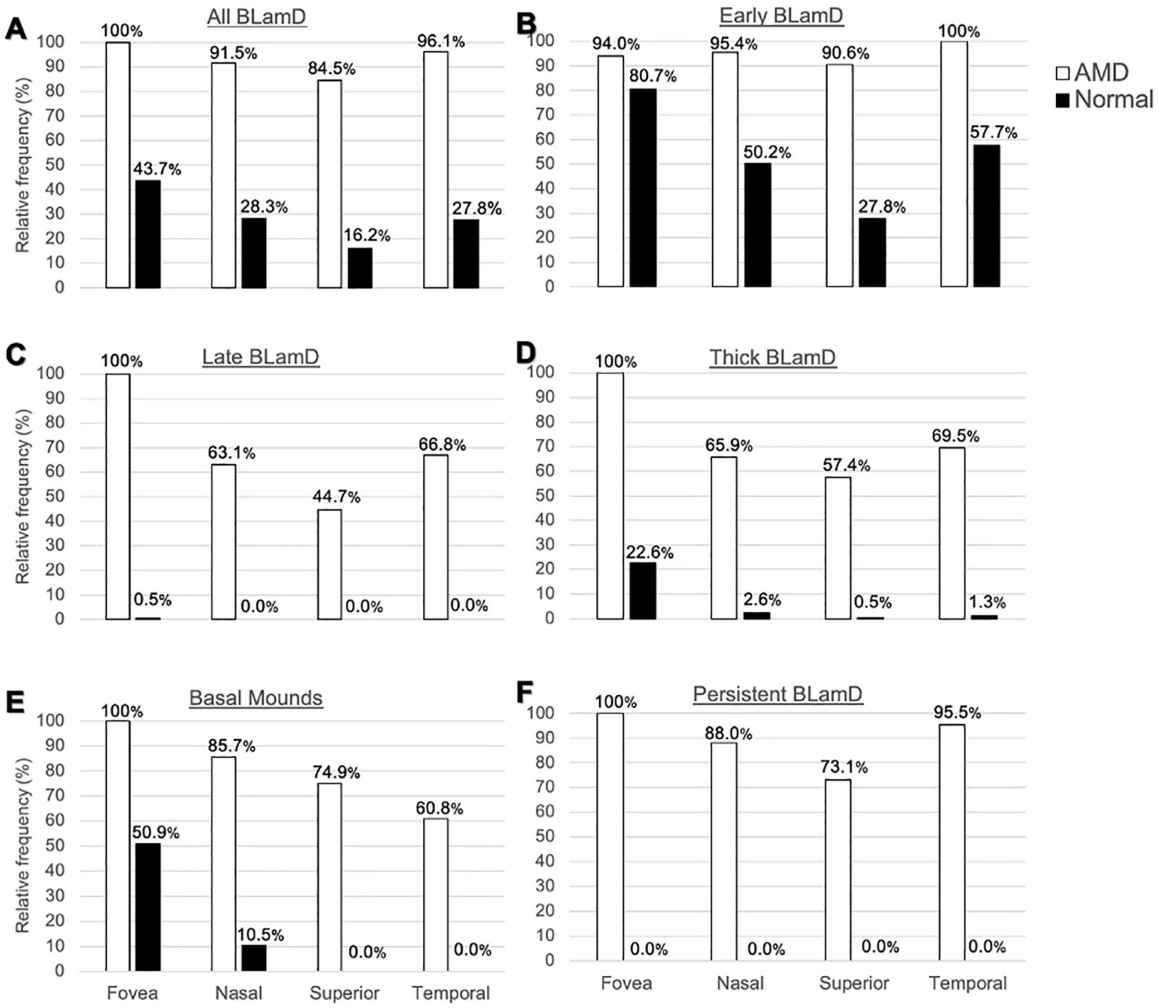

Figure 6. Topography of basal laminar deposit (BLamD) phenotypes. At predefined locations in the fovea and perifovea, the presence of any BLamD, early BLamD, late BLamD, thick BLamD, basal mounds, and persistent BLamD was assayed. Fovea and regions of perifovea was defined as described in the Methods section. Thick BLamD was defined as > 6.2 µm (half the thickness of the average RPE cell body).[39] Data are normalized to the most commonly encountered location for each diagnostic category. (**A, B**) In eyes with AMD, BLamD and early BLamD was widespread. (**C, D**) Late and thick BLamD are specific for AMD and frequently accumulate under the fovea. (**E**) Basal mounds cluster subfoveally, even in normal eyes.

eye and in AMD eyes (9.9, 8.1, and 7.6 µm for early to intermediate, GA, and NV eyes, respectively). These values represent lower bounds for this distance in vivo, which includes contents of the sub-RPE-BL space (e.g. drusen and fluid) as well.

Clinicopathologic Correlation

Figure 8 shows a multiscale clinicopathologic correlation of BLamD in a clinically documented eye with subfoveal nonexudative type 1 MNV. In vivo OCT B-scan acquired 16 months before the patient's death shows a large, central, SIRE and a split RPE-BL-BrM complex ("double-layer sign"; on the left, see Fig. 8A). By histology, we found that the SIRE on OCT B-scan corresponded to type 1 MNV (see Fig. 8B) with BLamD and a thin BrM, as well as a continuous and thick ellipsoid zone (see Figs. 8G, 8H). The split RPE-BL-BrM complex (see Fig. 8B) corresponded to a very thick BLamD and short photoreceptors (see Figs. 8E, 8F), without MNV. Areas without RPE elevation (see Fig. 8B) were seen to correspond to a continuous RPE layer with very thin BLamD and intact ELM (see Figs. 8C, 8D). Additionally, the hyper-reflective RPE-BrM band on OCT B-scan is noticeably thicker in both areas with RPE elevations due to thick late BLamD (see Figs. 8E–H).

Discussion

We provide a systematic and comprehensive histopathologic examination of the presence, morphology, thickness, and topography of BLamD across AMD stages, including normal aged eyes. Like the Sarks[17] we showed that central macula accumulates BLamD. By also examining nonfoveal regions we refined the relationship of BLamD with the neural retina. BLamD is the main contributor to thickening of the RPE-BL-BrM complex in AMD (aside from sub-RPE-BL material like drusen). Further, we show that BLamD, when thick, is visible in vivo with OCT in AMD. Our data can help refine models of pathogenesis and impact interpretation of preclinical data and clinical OCT.

Our data suggest that thickness of the RPE-BL complex in AMD is driven by the accumulation of BLamD. In contrast,

Table 4. Components of the Retinal Pigment Epithelium (RPE)-Basal Lamina-Bruch's Membrane (BrM) Complex

	Unremarkable	Early to Intermediate AMD	Geographic Atrophy	Neovascular AMD
All RPE measurements				
RPE thickness	12.5 (11.8, 14)	10.9 (10.0, 13.1)	7.1 (5.9, 8.7)	6.2 (3.1, 9.8)
BLamD thickness	0.3 (0, 1.1)	5.5 (3.1, 8.6)	4.1 (3.6, 7.0)	5.5 (3.1, 8.6)
BrM thickness	4.2 (3.7, 4.6)	4.4 (4.1, 4.8)	4.2 (4.0, 4.6)	3.5 (2.9, 3.9)
RPE + BLamD thickness	13.7 (12.5, 14.9)	16.4 (15.0, 20.1)	12.2 (9.7, 14.5)	10.7 (6.7, 16.8)
BLamD + BrM thickness	4.7 (4.1, 5.1)	9.9 (7.4, 13.4)	8.1 (7.1, 10.4)	7.6 (6.3, 11.6)
Excluding atrophy				
RPE thickness	12.5 (11.8, 14)	11.2 (10.0, 13.1)	12.7 (10.9, 13.1)	13.6 (11.4, 16.9)
BLamD thickness	0.3 (0, 1.1)	5.5 (3.0, 7.8)	4.1 (3.0, 8.3)	5.3 (2.9, 7.2)
BrM thickness	4.2 (3.7, 4.6)	4.4 (4.1, 4.8)	4.2 (3.5, 4.6)	3.6 (3.1, 4.0)
RPE + BLamD thickness	13.7 (12.5, 14.9)	16.8 (15.0, 19.8)	17.4 (15.4, 21.8)	18.7 (15.3, 23.2)
BLamD + BrM thickness	4.7 (4.1, 5.1)	9.9 (7.4, 12.8)	8.1 (7.4, 10.6)	9.1 (6.8, 11.3)

At predefined locations in the fovea and perifovea, thicknesses of the RPE, BLamD, and BrM were assayed (19–38 locations per eye), units are µm.

Areas of atrophy, defined as areas where RPE = 0, were either excluded or included.

Measurements within the same eye were averaged, and each eye was ranked.

Data represent median and interquartile range of the rank list.

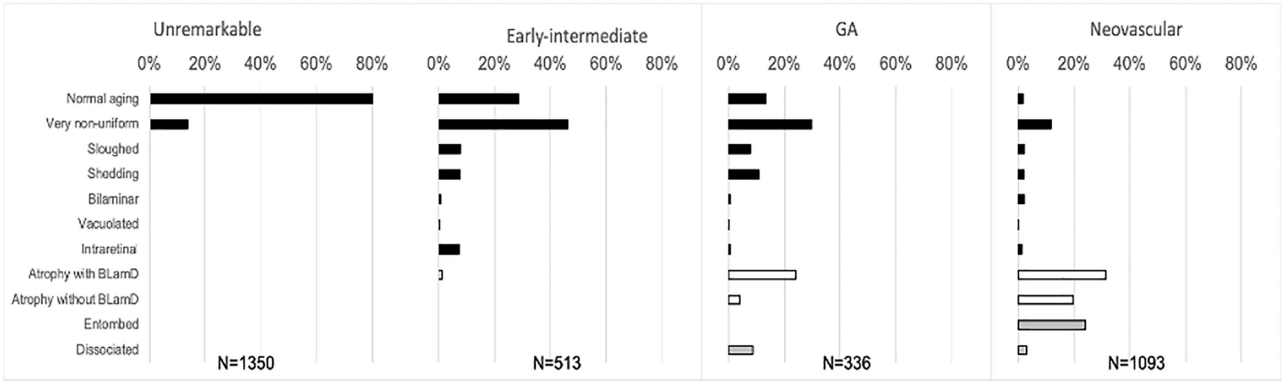

Figure 7. Phenotypes of retinal pigment epithelium (RPE) morphology in different stages of age-related macular degeneration (AMD). At predefined locations in the fovea and perifovea, RPE phenotypes were determined using the Project MACULA RPE grading system. Data represent percentage of measurements with a given phenotype, with degree of pathology increasing down the y axis. RPE appears more dysmorphic in early-intermediate AMD than in unremarkable eyes. Eyes with geographic atrophy and neovascular AMD have few RPE cells with normal architecture. Legend: *black bars*, epithelial; *white bars*, atrophic; *grey bars*, nonepithelial.

the three-layer BrM maintains its thickness except in NV AMD, where it thins (see Fig. 5). This thinning is accompanied by breakthroughs of pre-NV buds to form type 1 MNV.[19,35,36] To definitively separate BLamD from BrM over a wide area, we studied many eyes with high-resolution and high-magnification tissue visualization techniques. Previous major surveys (> 100 eyes) of age-related macular pathology used light microscopy of paraffin embedded tissue supplemented by transmission electron microscopy of small tissue blocks.[16,17,37–39] Other large surveys utilizing immunohistochemistry provided essential information about choriocapillaris degeneration,[40,41] of relevance to our model of AMD deposit formation (see below). W.R. Green considered BLamD part of BrM.[16] The Rotterdam group showed age-related accumulation of BLamD and prominent banded type VI collagen ($n = 145$).[29,39] Chong et al. reported thickness and foveal discontinuity of BrM elastic layer by electron microscopy ($n = 121$) but did not report BLamD or total BrM thickness.[42] Studies that report thickening of the RPE band or BrM in AMD may also include BLamD in their measurements and should thus be interpreted cautiously.

Our findings reaffirm that BLamD is a key histologic feature of AMD[11,29,38,43–46] first found in 1976 when S.H. Sarks categorized AMD severity by BLamD presence and abundance in paraffin histology.[37] Although thin and patchy BLamD are common in aged eyes,[47] BLamD in AMD is continuous (see Fig. 2), frequent (see Fig. 4), and thick (see Fig. 5). Certain BLamD phenotypes are markers of severe RPE pathology. According to the Sarks' clinicopathologic correlations, both thick and late BLamD were associated with vision loss.[17] In normal eyes, we never encountered late BLamD, and thick BLamD was graded in < 5% of locations (see Fig. 3). By contrast, BLamD thickness ranged up to 20 µm when underlying highly dysmorphic RPE (see Table 3). Late and thick BLamD are ultrastructurally distinct from early BLamD as well as more voluminous. Our current data do not resolve whether these two effects are due to altered contents, remodeling, or both. As elaborated below, evidence for altered and indeed regulated contents are the orderly and stereotypic structure of BLamD and the continuance of a thin native RPE-BL where RPE is present. Evidence for remodeling is the involvement of the TIMP3 gene.[45,48] Interestingly, median BLamD thickness in early to intermediate, GA, and NV AMD eyes (see Fig. 5) was 5.5 µm, 4.1 µm, and 5.3 µm, respectively. Because RPE produces and maintains BLamD components (e.g. fibulin

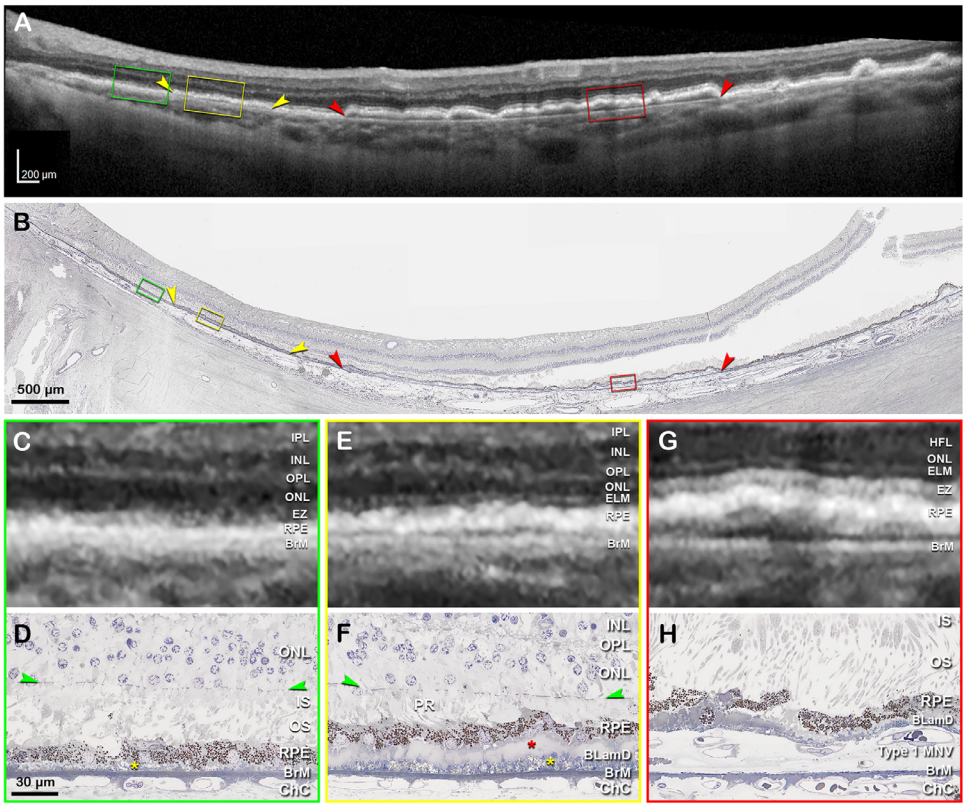

Figure 8. Clinicopathologic correlation of BLamD, compared to type 1 MNV. (**A**) Optical coherence tomography (OCT) B-scan 16 months before patient death shows a large, central, shallow irregular RPE elevation (SIRE; *red arrowheads*), and a split RPE-BL-BrM complex or "double-layer sign" on the left (*yellow arrowheads*). *Green, yellow, and red frames* are magnified in panels **C**, **E**, and **G**, respectively. (**B**) Panoramic view of histology shows type 1 macular neovascularization (MNV; *red arrowheads*), and a thick basal laminar deposit (BLamD; *yellow arrowhead*), exactly corresponding with the OCT B-scan. *Green, yellow, and red frames* are magnified in panel **D**, **F**, and **H**, respectively. (**C**) Magnified OCT B-scan shows an area without RPE-BL elevation. The ELM is visible on the left side. The EZ band is not continuous. (**D**) Magnified histologic image shows a continuous RPE layer with very thin BLamD (*yellow asterisk*), intact ELM, and dyslaminate ONL-HFL. (**E**) Magnified OCT B-scan shows an area with a split RPE-BL-BrM complex. The hyper-reflective RPE band is noticeably thicker, with a thin hyporeflective band between it and Bruch's membrane. The ELM is detectable. An EZ band is not discernible. (**F**) Magnified histologic image shows a continuous RPE layer and short photoreceptors (PRs). A very thick layer of BLamD, including early (*yellow asterisk*) and late (*red asterisk*) forms can be observed underneath the RPE. (**G**) Magnified OCT B-scan shows an area with a SIRE. The RPE-BL band is thickened and the EZ band is continuous and thick. **(H)** Magnified histologic image shows type 1 MNV between RPE with BLamD and a thin BrM. IPL, inner plexiform layer; INL, inner nuclear layer; OPL, outer plexiform layer; HFL, Henle fiber layer; ONL, outer nuclear layer; ELM, external limiting membrane; EZ, ellipsoid zone; RPE, retinal pigment epithelium; BL, basal lamina; BrM, Bruch's membrane; IS, inner segment; OS, outer segment; ChC, choriocapillaris. Scale bar in **D** applies to **D**, **F**, and **H**.

3),[49,50] a certain level of RPE functionality is needed to synthesize and maintain BLamD, as suggested for drusen[51] and subretinal drusenoid deposits (SDDs).[31] In areas of long-standing RPE atrophy, BLamD persists and looks ragged (see Fig. 2),[52] consistent with a loss of maintenance.

Within BLamD, we observed BMounds (see Fig. 3).[48,53] These drusen-like structures contain cholesterol-rich material (Figs. 3F–3H of reference 54) and uniquely exist in BLamD itself rather than in the sub-RPE-BL space (see Fig. 1). The forerunner of BMounds (and drusen) is electron-dense lipid-rich material seen within BLamD and located internal to the thin native RPE-BL (Figs. 2 and 4 of reference 48 Figs. 3 and 4 of reference 45, and Figs. 1–4 of reference 17) This material was attributed to lipoprotein particles rather than degenerating basal infoldings due to the high electron density relative to adjacent cell membranes and actual particles seen in well-preserved human specimens[45] as well as in mouse models.[55] Appearing as focal elevations, continuous swaths, or complex structures with calcification (see Fig. 3), BMounds' ultrastructure, morphology, and inferred lifecycle suggests a similar pathophysiology to soft drusen. Whether drusen or BMounds form may depend on whether BrM or BLamD is the proximal lipid-retentive structure, respectively. BMounds can appear alongside drusen, or they may constitute the primary form of lipoprotein-rich debris in some patients, according to the Sarks. In "drusen-independent AMD," patients present at older ages with greater vision loss but a lower risk for type 1 MNV compared to patients with drusen.[17] Future studies with advanced OCT may address whether BMounds are distinguishable from dome-shaped soft drusen.

Our study examined the spatial topography of BLamD, finding that the advanced phenotypes (thick, late, and BMounds) are most common in the foveal region (see Fig. 6). Hypothesizing that deposit formation has a cellular basis in neurosensory retina, we used a coordinate system anchored on the rod-free zone to study lesion topography.[56,57] High-risk drusen and BLinD concentrate in the central subfield of the Early Treatment Diabetic Retinopathy Study (ETDRS) grid and fall off sharply within

1.5 mm eccentricity.[25,26,58,59] The subfoveal predilection of BMounds in normal eyes supports Sarks' hypothesis that BLamD is a major contributor to drusen accumulation,[15,17] as follows. The best supported model of drusen formation suggests a lifelong release of lipoproteins by the RPE to offload unneeded lipids to the circulation. It is further proposed that a major source of these unneeded lipids is plasma HDL that deliver xanthophyll carotenoids destined for foveal Muller glia and cones.[60] Our data support a model in which a dysfunctional barrier due to aging BrM and choriocapillaris sequesters lipids first in BrM, then the sub-RPE-BL space (drusen),[61] and then in BLamD as BMounds. In contrast, SDD in AMD track rod photoreceptor topography, and in these regions BLamD was reported as thinner than it is in areas with BLinD (4.2 vs. 6.3 µm).[18] Our current data do not allow us to refine the topographic relationship of BLamD with SDD, because we did not sample areas with the highest rod densities (3–5 mm eccentricity).

BLamD accumulation may have a genetic basis. Some AMD risk alleles code for extracellular matrix proteins[62] found in BLamD: complement factors, EFEMP, C1QTNF5, and TIMP3.[13,14,63,64] Alterations to these proteins result in early onset maculopathies with thick BLamD, drusen, BrM pathology, and atrophic and NV complications. These include Sorsby fundus dystrophy (TIMP3),[14,65] late-onset retinal degeneration (C1QTNF5) ,[66,67] Malattia Leventinese/ Doyne's honeycomb retinal dystrophy (EFEMP1),[50,68,69] dense deposit disease / membranoproliferative glomerulonephritis type II (C3 / CFH),[70,71] and possibly Martinique crinkled retinal pigment epitheliopathy (MAPKAP3).[72–74] These genes are distinct from those impacting the three-layer BrM (pseudoxanthoma elasticum, ABCC6).[75]

BLamD in AMD and C1QTNF5 disease contain histochemically- and ultrastructurally-identified lipid and apolipoprotein B immunoreactivity, thus implicating BLamD as a lipid retentive matrix.[45,54,76] Some mouse strains exhibit thin BLamD, and, to date, only models involving the genes listed above have thick BLamD.[66,77] Aged monkeys may naturally exhibit soft drusen, but lack BLamD and do not progress to atrophy or NV,[78] suggesting that BLamD is required for drusen that progress. Indeed, BLamD may share some of the pathophysiology postulated for drusen, with important differences. Our data show that, on average, BLamD doubles the diffusion distance between the RPE and choriocapillaris relative to three-layer BrM alone (see Table 4). Modification of lipoproteins resulting in pro-inflammatory lipids may also occur in thick BLamD, especially if BMounds are present.

BLamD's basement membrane (BM)-like qualities may also serve protective functions, similar to BM hypertrophy in other diseases (e.g. alveolar BM in asthma[79] and glomerular BM in nephropathy[80]). BLamD may protect the RPE and outer retina from pro-inflammatory drusen and BLinD.[81] Persistent BLamD may serve as a scaffold onto which RPE can migrate, adhere to, and repopulate focal areas of atrophy.[82] In NV AMD, BLamD may tamponade type 1 MNV from breaking through RPE and reaching the outer retina (see Fig. 2), a role distinct from drusen material, which acts as a cleavage plane allowing vascular expansion. An open question is whether BLamD shares anti-angiogenic properties of native BMs via endorepellin domain of heparan sulfate proteoglycans and type 18 collagen.[9,83]

We directly showed with histology of a clinically documented eye that BLamD can be visible and differentiable from type 1 MNV on OCT. A very thick BLamD appeared as a split RPE-BL-BrM complex or "double-layer sign" (i.e. a thick, uniform hyperreflective band with a thin hyporeflective band separating it from BrM; Fig. 8). In contrast, type 1 MNV in the same eye appeared as a SIRE with heterogeneously reflective material between it and BrM.[19,84] Distinguishing a SIRE from thick BLamD may be important in assessing an eye's risk for conversion to exudative MNV.[19] Our observations overall expand the set of OCT signatures attributed to BLamD. Thick BLamD accounts for "splitting of the fourth hyper-reflective band" in areas of rapidly progressive GA[85] and some inherited retinopathies.[67,73,86,87] In areas of RPE atrophy in AMD, persistent BLamD may appear as an undulating hyper-reflective line ("outer retinal corrugations[52] and "plateau"[88]). The reflectivity of persistent BLamD is attributed to the loss of RPE shadowing and altered BLamD composition (due to loss of RPE maintenance, see above). Persistent BLamD has been erroneously considered the outer plexiform layer by some authors, possibly contributing to a false impression of viable photoreceptors in atrophic areas.[89,90] Thus, we encourage developers of automated OCT segmentation strategies[91] and nomenclatures[92,93] to incorporate the presence of BLamD, especially in atrophy. Further, because the fourth hyper-reflective outer retinal band of the consensus lexicon correlates to the RPE-BL-BrM complex[94] (see Fig. 1), the nomenclature for normal eyes should also be updated to include the RPE-BL; we have suggested the term RBB.[95]

Our study has strengths: near-ultrastructural resolution over a wide area, unbiased sampling, large sample size, donor tissue with short death-to-preservation time, quantitative layer segmentation, attention to retinal topography, and methods to preserve extracellular lipids. Limitations include under-representation of intermediate AMD eyes with large drusen, under-representation of retinal regions where SDD is abundant, lack of molecular identifications due to glutaraldehyde fixation, artifactual tissue detachments, and the subjective nature of histology. Open questions requiring future electron microscopic analysis are the fate of RPE basal infoldings, a fourth reflective band component (see Fig. 1), and whether native RPE-BL is part of persistent BLamD in areas lacking RPE. Nevertheless, our data lend support to concepts worthy of further testing (i.e. that BLamD thickness and phenotype vary across AMD stages, RPE phenotype, and retinal location, and that thickness of the three-layer BrM is stable except in NV). We found that the addition and expansion of BLamD accumulation is an important histopathologic change to the RPE-BL-BrM complex during the transition to AMD. BLamD's omnipresence and subfoveal abundance suggests important roles in AMD progression, including promoting high-risk drusen and protecting from exudation. Finally, we show that BLamD is directly visible in vivo via OCT. This capability can enhance interpretation of clinical imaging for differential diagnosis and guide ongoing studies of AMD natural history in genotyped patients (NCT04112667 [ALSTAR2], NCT03349801 [MACUSTAR], and NCT03092492 [ARIS]).

Acknowledgments

The authors thank David Fisher for the graphics in Figure 1.

The Project MACULA website and the recovery of human donor eyes for research has been supported by National Institutes of Health (NIH) grants R01EY06019 and P30 EY003039, EyeSight Foundation of Alabama, International Retinal Research

Foundation, Edward N. and Della L. Thome Foundation, the Arnold and Mabel Beckman Initiative for Macular Research, and Research to Prevent Blindness. Purchase of the slide scanner was made possible by the Carl G. and Pauline Buck Trust.

Previously presented: Annual meeting of Association for Research in Vision and Ophthalmology, 2019.

Disclosure: **A.A. Sura**, None; **L. Chen**, None; **J.D. Messinger**, None; **T.A. Swain**, None; **G. McGwin Jr.**, None; **K.B. Freund**, Optovue (C), Heidelberg Engineering (C), Bayer (C), Zeiss (C), Allergan (C), and Novartis (C), and Genentech/Roche (F). **C.A. Curcio**, Heidelberg Engineering and Genentech/Hoffman LaRoche (F), MacRegen Inc (I)

References

1. Flaxman SR, Bourne RRA, Resnikoff S, et al. Global causes of blindness and distance vision impairment 1990–2020: a systematic review and meta-analysis. *Lancet Glob Health*. 2017;5:e1221–e1234.
2. Comparison of Age-related Macular Degeneration Treatments Trials Research Group,Maguire MG, Martin DF, et al. Five-year outcomes with anti-vascular endothelial growth factor treatment of neovascular age-related macular degeneration: the comparison of age-related macular degeneration treatments trials. *Ophthalmology*. 2016;123:1751–1761.
3. Age-Related Eye Disease Study 2 Research Group. Lutein + zeaxanthin and omega-3 fatty acids for age-related macular degeneration: the Age-Related Eye Disease Study 2 (AREDS2) randomized clinical trial. *JAMA*. 2013;309:2005–2015.
4. Staurenghi G, Sadda S, Chakravarthy U, Spaide RF, International Nomenclature for Optical Coherence Tomography (IN OCT) Panel. Proposed lexicon for anatomic landmarks in normal posterior segment spectral-domain optical coherence tomography: the IN*OCT consensus. *Ophthalmology*. 2014;121:1572–1578.
5. Gass JDM. *Stereoscopic atlas of macular diseases: diagnosis and treatment*. St. Louis, MO: Mosby; 1997.
6. Bressler SB, Bressler NM, Sarks SH, Sarks JP. Age-related macular degeneration: nonneovascular early AMD, intermediate AMD, and geographic atrophy. In: Ryan SJ (ed), *Retina*. St. Louis, MO: Mosby; 2006:1041–1074.
7. Halfter W, Oertle P, Monnier CA, et al. New concepts in basement membrane biology. *FEBS J*. 2015;282:4466–4479.
8. Mak KM, Mei R. Basement membrane type IV collagen and laminin: an overview of their biology and value as fibrosis biomarkers of liver disease. *Anat Rec (Hoboken)*. 2017;300:1371–1390.
9. Pozzi A, Yurchenco PD, Iozzo RV. The nature and biology of basement membranes. *Matrix Biol*. 2017;57-58:1–11.
10. Chen L, Miyamura N, Ninomiya Y, Handa JT. Distribution of the collagen IV isoforms in human Bruch's membrane. *Br J Ophthalmol*. 2003;87:212–215.
11. Loffler KU, Lee WR. Basal linear deposit in the human macula. *Graefes Arch Clin Exp Ophthalmol*. 1986;224:493–501.
12. Marshall GE, Konstas AG, Reid GG, Edwards JG, Lee WR. Type IV collagen and laminin in Bruch's membrane and basal linear deposit in the human macula. *Br J Ophthalmol*. 1992;76:607–614.
13. Knupp C, Munro PM, Luther PK, Ezra E, Squire JM. Structure of abnormal molecular assemblies (collagen VI) associated with human full thickness macular holes. *J Struct Biol*. 2000;129:38–47.
14. Knupp C, Chong NHV, Munro PMG, Luthert PJ, Squire JM. Analysis of the collagen VI assemblies associated with Sorsby's fundus dystrophy. *J Struct Biol*. 2002;137(1-2):31–40.
15. Sarks SH. Council Lecture: drusen and their relationship to senile macular degeneration. *Aust J Ophthalmol*. 1980;8:117–130.
16. Green WR, Enger C. Age-related macular degeneration histopathologic studies. The 1992 Lorenz E. Zimmerman Lecture. *Ophthalmology*. 1993;100:1519–1535.
17. Sarks S, Cherepanoff S, Killingsworth M, Sarks J. Relationship of basal laminar deposit and membranous debris to the clinical presentation of early age-related macular degeneration. *Invest Ophthalmol Vis Sci*. 2007;48:968–977.
18. Curcio CA, Messinger JD, Sloan KR, McGwin G, Medeiros NE, Spaide RF. Subretinal drusenoid deposits in non-neovascular age-related macular degeneration: morphology, prevalence, topography, and biogenesis model. *Retina*. 2013;33:265–276.
19. Chen L, Messinger JD, Sloan KR, et al. Nonexudative macular neovascularization supporting outer retina in age-related macular degeneration: a clinicopathologic correlation. *Ophthalmology*. 2020;127:931–947.
20. Biesemeier A, Taubitz T, Julien S, Yoeruek E, Schraermeyer U. Choriocapillaris breakdown precedes retinal degeneration in age-related macular degeneration. *Neurobiol Aging*. 2014;35:2562–2573.
21. Curcio CA, Zanzottera EC, Ach T, Balaratnasingam C, Freund KB. Activated retinal pigment epithelium, an optical coherence tomography biomarker for progression in age-related macular degeneration. *Invest Ophthalmol Vis Sci*. 2017;58:BIO211–BIO226.
22. Li M, Jia C, Kazmierkiewicz KL, et al. Comprehensive analysis of gene expression in human retina and supporting tissues. *Hum Mol Genet*. 2014;23:4001–4014.
23. Guyton JR, Klemp KF. Ultrastructural discrimination of lipid droplets and vesicles in atherosclerosis: value of osmium-thiocarbohydrazide-osmium and tannic acid-paraphenylenediamine techniques. *J Histochem Cytochem*. 1988;36:1319–1328.
24. Curcio CA, Sloan KR, Kalina RE, Hendrickson AE. Human photoreceptor topography. *J Comp Neurol*. 1990;292:497–523.
25. Wang JJ, Rochtchina E, Lee AJ, et al. Ten-year incidence and progression of age-related maculopathy: the Blue Mountains Eye Study. *Ophthalmology*. 2007;114:92–98.
26. Klein R, Klein BE, Knudtson MD, Meuer SM, Swift M, Gangnon RE. Fifteen-year cumulative incidence of age-related macular degeneration: the Beaver Dam Eye Study. *Ophthalmology*. 2007;114:253–262.
27. Steinberg JS, Auge J, Jaffe GJ, et al. Longitudinal analysis of reticular drusen associated with geographic atrophy in age-related macular degeneration. *Invest Ophthalmol Vis Sci*. 2013;54:4054–4060.
28. Schindelin J, Arganda-Carreras I, Frise E, et al. Fiji: an open-source platform for biological-image analysis. *Nat Methods*. 2012;9:676–682.
29. van der Schaft TL, Mooy CM, de Bruijn WC, Oron FG, Mulder PG, de Jong PT. Histologic features of the early stages of age-related macular degeneration. A statistical analysis. *Ophthalmology*. 1992;99:278–286.
30. Zanzottera EC, Messinger JD, Ach T, Smith RT, Freund KB, Curcio CA. The Project MACULA retinal pigment epithelium grading system for histology and optical coherence tomography in age-related macular degeneration. *Invest Ophthalmol Vis Sci*. 2015;56:3253–3268.
31. Chen L, Messinger JD, Zhang Y, Spaide RF, Freund KB, Curcio CA. Subretinal drusenoid deposit in age-related macular degeneration: histologic insights into initiation, progression to atrophy, and imaging. *Retina*. 2020;40:618–631.

Investigative Ophthalmology & Visual Science

32. Mullins RF, Johnson MN, Faidley EA, Skeie JM, Huang J. Choriocapillaris vascular dropout related to density of drusen in human eyes with early age-related macular degeneration. *Invest Ophthalmol Vis Sci*. 2011;52:1606–1612.
33. McLeod DS, Grebe R, Bhutto I, Merges C, Baba T, Lutty GA. Relationship between RPE and choriocapillaris in age-related macular degeneration. *Invest Ophthalmol Vis Sci*. 2009;50:4982–4991.
34. van den Brink H, Zwiers A, Switzer AR, et al. Cortical microinfarcts on 3T magnetic resonance imaging in cerebral amyloid angiopathy. *Stroke*. 2018;49:1899–1905.
35. Killingsworth MC. Angiogenesis in early choroidal neovascularization secondary to age-related macular degeneration. *Graefes Arch Clin Exp Ophthalmol*. 1995;233:313–323.
36. Seddon JM, McLeod DS, Bhutto IA, et al. Histopathological insights into choroidal vascular loss in clinically documented cases of age-related macular degeneration. *JAMA Ophthalmol*. 2016;134:1272–1280.
37. Sarks SH. Ageing and degeneration in the macular region: a clinico-pathological study. *Br J Ophthalmol*. 1976;60:324–341.
38. Spraul CW, Lang GE, Grossniklaus HE. Morphometric analysis of the choroid, Bruch's membrane, and retinal pigment epithelium in eyes with age-related macular degeneration. *Invest Ophthalmol Vis Sci*. 1996;37:2724–2735.
39. van der Schaft TL, de Bruijn WC, Mooy CM, de Jong PT. Basal laminar deposit in the aging peripheral human retina. *Graefes Arch Clin Exp Ophthalmol*. 1993;231:470–475.
40. Mullins RF, Schoo DP, Sohn EH, et al. The membrane attack complex in aging human choriocapillaris: relationship to macular degeneration and choroidal thinning. *Am J Pathol*. 2014;184:3142–3153.
41. Sohn EH, Flamme-Wiese MJ, Whitmore SS, Wang K, Tucker BA, Mullins RF. Loss of CD34 expression in aging human choriocapillaris endothelial cells. *PLoS One*. 2014;9:e86538.
42. Chong NH, Keonin J, Luthert PJ, et al. Decreased thickness and integrity of the macular elastic layer of Bruch's membrane correspond to the distribution of lesions associated with age-related macular degeneration. *Am J Pathol*. 2005;166:241–251.
43. Sarks SH. The aging eye. *Med J Aust*. 1975;2:602–604.
44. Feeney-Burns L, Ellersieck MR. Age-related changes in the ultrastructure of Bruch's membrane. *Am J Ophthalmol*. 1985;100:686–697.
45. Curcio CA, Presley JB, Millican CL, Medeiros NE. Basal deposits and drusen in eyes with age-related maculopathy: evidence for solid lipid particles. *Exp Eye Res*. 2005;80:761–775.
46. Grossniklaus HE, Nickerson JM, Edelhauser HF, Bergman LA, Berglin L. Anatomic alterations in aging and age-related diseases of the eye. *Invest Ophthalmol Vis Sci*. 2013;54:ORSF23–27.
47. Ramrattan RS, van der Schaft TL, Mooy CM, de Bruijn WC, Mulder PG, de Jong PT. Morphometric analysis of Bruch's membrane, the choriocapillaris, and the choroid in aging. *Invest Ophthalmol Vis Sci*. 1994;35:2857–2864.
48. Curcio CA, Millican CL. Basal linear deposit and large drusen are specific for early age-related maculopathy. *Arch Ophthalmol*. 1999;117:329–339.
49. Galloway CA, Dalvi S, Hung SSC, et al. Drusen in patient-derived hiPSC-RPE models of macular dystrophies. *Proc Natl Acad Sci USA*. 2017;114:E8214–E8223.
50. Marmorstein LY, Munier FL, Arsenijevic Y, et al. Aberrant accumulation of EFEMP1 underlies drusen formation in Malattia Leventinese and age-related macular degeneration. *Proc Natl Acad Sci USA*. 2002;99:13067–13072.
51. Balaratnasingam C, Yannuzzi LA, Curcio CA, et al. Associations between retinal pigment epithelium and drusen volume changes during the lifecycle of large drusenoid pigment epithelial detachments. *Invest Ophthalmol Vis Sci*. 2016;57:5479–5489.
52. Ooto S, Vongkulsiri S, Sato T, Suzuki M, Curcio CA, Spaide RF. Outer retinal corrugations in age-related macular degeneration. *JAMA Ophthalmology*. 2014;132(7):806–813.
53. Sarks JP, Sarks SH, Killingsworth MC. Evolution of geographic atrophy of the retinal pigment epithelium. *Eye (Lond)*. 1988;2(Pt 5):552–577.
54. Curcio CA, Presley JB, Malek G, Medeiros NE, Avery DV, Kruth HS. Esterified and unesterified cholesterol in drusen and basal deposits of eyes with age-related maculopathy. *Exp Eye Res*. 2005;81:731–741.
55. Jiang M, Esteve-Rudd J, Lopes VS, et al. Microtubule motors transport phagosomes in the RPE, and lack of KLC1 leads to AMD-like pathogenesis. *J Cell Biol*. 2015;210:595–611.
56. Bogunovic H, Montuoro A, Baratsits M, et al. Machine learning of the progression of intermediate age-related macular degeneration based on OCT imaging. *Invest Ophthalmol Vis Sci*. 2017;58:BIO141–BIO150.
57. Waldstein SM, Vogl WD, Bogunovic H, Sadeghipour A, Riedl S, Schmidt-Erfurth U. Characterization of drusen and hyperreflective foci as biomarkers for disease progression in age-related macular degeneration using artificial intelligence in optical coherence tomography. *JAMA Ophthalmol*. 2020;138:740–747.
58. Wang Q, Chappell RJ, Klein R, et al. Pattern of age-related maculopathy in the macular area. The Beaver Dam Eye Study. *Invest Ophthalmol Vis Sci*. 1996;37:2234–2242.
59. Joachim N, Mitchell P, Burlutsky G, Kifley A, Wang JJ. The incidence and progression of age-related macular degeneration over 15 years: the Blue Mountains Eye Study. *Ophthalmology*. 2015;122:2482–2489.
60. Curcio CA. Antecedents of soft drusen, the specific deposits of age-related macular degeneration, in the biology of human macula. *Invest Ophthalmol Vis Sci*. 2018;59:AMD182–AMD194.
61. Curcio CA, Johnson M. Structure, function, and pathology of Bruch's membrane. *Retina Fifth Edition*. New York, NY: Elsevier; 2012.
62. Fritsche LG, Igl W, Bailey JN, et al. A large genome-wide association study of age-related macular degeneration highlights contributions of rare and common variants. *Nat Genet*. 2016;48:134–143.
63. Lommatzsch A, Hermans P, Muller KD, Bornfeld N, Bird AC, Pauleikhoff D. Are low inflammatory reactions involved in exudative age-related macular degeneration? Morphological and immunhistochemical analysis of AMD associated with basal deposits. *Graefes Arch Clin Exp Ophthalmol*. 2008;246:803–810.
64. Garland DL, Fernandez-Godino R, Kaur I, et al. Mouse genetics and proteomic analyses demonstrate a critical role for complement in a model of DHRD/ML, an inherited macular degeneration. *Hum Mol Genet*. 2014;23:52–68.
65. Weber BH, Vogt G, Pruett RC, Stohr H, Felbor U. Mutations in the tissue inhibitor of metalloproteinases-3 (TIMP3) in patients with Sorsby's fundus dystrophy. *Nat Genet*. 1994;8:352–356.
66. Hayward C, Shu X, Cideciyan AV, et al. Mutation in a short-chain collagen gene, CTRP5, results in extracellular deposit formation in late-onset retinal degeneration: a genetic model for age-related macular degeneration. *Hum Mol Genet*. 2003;12:2657–2667.

Investigative Ophthalmology & Visual Science

67. Milam AH, Curcio CA, Cideciyan AV, et al. Dominant late-onset retinal degeneration with regional variation of sub-retinal pigment epithelium deposits, retinal function, and photoreceptor degeneration. *Ophthalmology*. 2000;107:2256–2266.
68. Stone EM, Lotery AJ, Munier FL, et al. A single EFEMP1 mutation associated with both Malattia Leventinese and Doyne honeycomb retinal dystrophy. *Nat Genet*. 1999;22:199–202.
69. Marmorstein L. Association of EFEMP1 with malattia leventinese and age-related macular degeneration: a mini-review. *Ophthalmic Genet*. 2004;25:219–226.
70. Song D, Mohammed I, Bhuyan R, et al. Retinal basal laminar deposits in complement fH/fP mouse model of dense deposit disease. *Invest Ophthalmol Vis Sci*. 2018;59(8):3405–3415.
71. Cunningham A, Kotagiri A. A long history of dense deposit disease. *BMC Ophthalmol*. 2018;18:228.
72. Jean-Charles A, Cohen SY, Merle H, Quentel G, Legargasson JF, Gaudric A. Martinique (West Indies) crinkled retinal pigment epitheliopathy: clinical description. *Retina*. 2013;33:1041–1048.
73. Jean-Charles A, Merle H, Audo I, et al. Martinique crinkled retinal pigment epitheliopathy: clinical stages and pathophysiologic insights. *Ophthalmology*. 2016;123(10):2196–2204.
74. Meunier I, Lenaers G, Bocquet B, et al. A dominant mutation in MAPKAPK3, an actor of p38 signaling pathway, causes a new retinal dystrophy involving Bruch's membrane and retinal pigment epithelium. *Hum Mol Genet*. 2016;25(5):916–926.
75. Bergen AA, Plomp AS, Schuurman EJ, et al. Mutations in ABCC6 cause pseudoxanthoma elasticum. *Nat Genet*. 2000;25:228–231.
76. Curcio CA, Johnson M, Rudolf M, Huang JD. The oil spill in ageing Bruch membrane. *Br J Ophthalmol*. 2011;95(12):1638–1645.
77. Chekuri A, Zientara-Rytter K, Soto-Hermida A, et al. Late-onset retinal degeneration pathology due to mutations in CTRP5 is mediated through HTRA1. *Aging Cell*. 2019;18:e13011.
78. Yiu G, Chung SH, Mollhoff IN, et al. Long-term evolution and remodeling of soft drusen in Rhesus Macaques. *Invest Ophthalmol Vis Sci*. 2020;61:32.
79. Castro-Rodriguez JA, Saglani S, Rodriguez-Martinez CE, Oyarzun MA, Fleming L, Bush A. The relationship between inflammation and remodeling in childhood asthma: a systematic review. *Pediatr Pulmonol*. 2018;53:824–835.
80. Han Q, Zhu H, Chen X, Liu Z. Non-genetic mechanisms of diabetic nephropathy. *Front Med*. 2017;11:319–332.
81. Datta S, Cano M, Ebrahimi K, Wang L, Handa JT. The impact of oxidative stress and inflammation on RPE degeneration in non-neovascular AMD. *Prog Retin Eye Res,* 2017;60:201–218.
82. Molina-Pallete R, Andreu-Fenoll M, Gallego-Pinazo R, Dolz-Marco R. Atypical healing in a case with retinal pigment epithelium apertures. *Retin Cases Brief Rep*, https://doi.org/10.1097/ICB.0000000000000789.
83. Gubbiotti MA, Neill T, Iozzo RV. A current view of perlecan in physiology and pathology: a mosaic of functions. *Matrix Biol*. 2017;57–58:285–298.
84. Spaide RF, Jaffe GJ, Sarraf D, et al. Consensus nomenclature for reporting neovascular age-related macular degeneration data: consensus on Neovascular Age-Related Macular Degeneration Nomenclature Study Group. *Ophthalmology*. 2020;127:616–636.
85. Fleckenstein M, Schmitz-Valckenberg S, Martens C, et al. Fundus autofluorescence and spectral-domain optical coherence tomography characteristics in a rapidly progressing form of geographic atrophy. *Invest Ophthalmol Vis Sci*. 2011;52:3761–3766.
86. Cukras C, Flamendorf J, Wong WT, Ayyagari R, Cunningham D, Sieving PA. Longitudinal structural changes in late-onset retinal degeneration. *Retina*. 2016;36:2348–2356.
87. Gliem M, Muller PL, Mangold E, et al. Sorsby Fundus dystrophy: novel mutations, novel phenotypic characteristics, and treatment outcomes. *Invest Ophthalmol Vis Sci*. 2015;56:2664–2676.
88. Tan ACS, Astroz P, Dansingani KK, et al. The evolution of the plateau, an optical coherence tomography signature seen in geographic atrophy. *Invest Ophthalmol Vis Sci*. 2017;58:2349–2358.
89. Sayegh RG, Kiss CG, Simader C, et al. A systematic correlation of morphology and function using spectral domain optical coherence tomography and microperimetry in patients with geographic atrophy. *Br J Ophthalmol*. 2014;98:1050–1055.
90. Querques G, Capuano V, Frascio P, Zweifel S, Georges A, Souied EH. Wedge-shaped subretinal hyporeflectivity in geographic atrophy. *Retina*. 2015;35:1735–1742.
91. Wu Z, Ayton LN, Luu CD, Guymer RH. Relationship between retinal microstructures on optical coherence tomography and microperimetry in age-related macular degeneration. *Ophthalmology*. 2014;121:1445–1452.
92. Sleiman K, Veerappan M, Winter KP, et al. Optical coherence tomography predictors of risk for progression to non-neovascular atrophic age-related macular degeneration. *Ophthalmology*. 2017;124:1764–1777.
93. Folgar FA, Yuan EL, Sevilla MB, et al. Drusen volume and retinal pigment epithelium abnormal thinning volume predict 2-year progression of age-related macular degeneration. *Ophthalmology*. 2016;123:39–50 e31.
94. Spaide RF, Curcio CA. Anatomical correlates to the bands seen in the outer retina by optical coherence tomography: literature review and model. *Retina*. 2011;31:1609–1619.
95. Balaratnasingam C, Hoang QV, Inoue M, et al. Clinical characteristics, choroidal neovascularization, and predictors of visual outcomes in acquired vitelliform lesions. *Am J Ophthalmol*. 2016;172:28–38.
96. Li M, Dolz-Marco R, Huisingh C, et al. Clinicopathologic correlation of geographic atrophy secondary to age-related macular degeneration. *Retina*. 2019;39:802–816.
97. Pollreisz A, Messinger JD, Sloan KR, et al. Visualizing melanosomes, lipofuscin, and melanolipofuscin in human retinal pigment epithelium using serial block face scanning electron microscopy. *Exp Eye Res*. 2018;166:131–139.
98. Pollreisz A, Neschi M, Sloan KR, et al. Atlas of human retinal pigment epithelium organelles significant for clinical imaging. *Invest Ophthalmol Vis Sci*. 2020;61:13.
99. Shirazi MF, Brunner E, Laslandes M, Pollreisz A, Hitzenberger CK, Pircher M. Visualizing human photoreceptor and retinal pigment epithelium cell mosaics in a single volume scan over an extended field of view with adaptive optics optical coherence tomography. *Biomed Opt Express*. 2020;11:4520–4535.
100. Lee B, Chen S, Moult EM, et al. High-speed, ultrahigh-resolution spectral-domain OCT with extended imaging range using reference arm length matching. *Transl Vis Sci Technol*. 2020;9:12.
101. Cuenca N, Ortuno-Lizaran I, Pinilla I. Cellular characterization of OCT and outer retinal bands using specific immunohistochemistry markers and clinical implications. *Ophthalmology*. 2018;125:407–422.

Investigative Ophthalmology & Visual Science

102. Gass JDM. Pathogenesis of disciform detachment of the neuroepithlium: senile disciform macular degeneration. *Am J Ophthalmol*. 1967;63:45–72.
103. Penfold PL, Killingsworth MC, Sarks SH. Senile macular degeneration: the involvement of immunocompetent cells. *Graefes Arch Clin Exp Ophthalmol*. 1985;223:69–76.
104. Spaide RF, Curcio CA. Drusen characterization with multimodal imaging. *Retina*. 2010;30:1441–1454.
105. Gass JDM. *Stereoscopic Atlas of Macular Diseases. Diagnosis and Treatment*. St. Louis, MO: C.V. Mosby; 1977.
106. Balaratnasingam C, Cherepanoff S, Dolz-Marco R, et al. Cuticular drusen: clinical phenotypes and natural history defined using multimodal imaging. *Ophthalmology*. 2018;125:100–118.

Investigative Ophthalmology & Visual Science